Density profiles and solvation forces for a Yukawa fluid in a slit pore

S. Karanikas,[1] J. Dzubiella,[2] A. Moncho-Jordá,[3] and A. A. Louis[4,a)]
[1]*Molecular Thermodynamics and Modelling of Materials Laboratory, Institute of Physical Chemistry, National Center for Scientific Research "Demokritos," GR-153 10 Aghia Paraskevi, Attikis, Greece*
[2]*Physik Department (T37), Technische Universität München, James Franck Strasse, 85748 Garching, Germany*
[3]*Departamento de Física Aplicada, Universidad de Granada, Facultad de Ciencias, Campus Fuentenueva S/N, 18071 Granada, Spain*
[4]*Rudolf Peierls Centre for Theoretical Physics, 1 Keble Road, Oxford OX1 3NP, United Kingdom*

(Received 2 November 2007; accepted 17 April 2008; published online 27 May 2008)

The effect of varying wall-particle and particle-particle interactions on the density profiles near a single wall and the solvation forces between two walls immersed in a fluid of particles is investigated by grand canonical Monte Carlo simulations. Attractive and repulsive particle-particle and particle-wall interactions are modeled by a versatile hard-core Yukawa form. These simulation results are compared to theoretical calculations using the hypernetted chain integral equation technique, as well as with fundamental measure density functional theory (DFT), where particle-particle interactions are either treated as a first order perturbation using the radial distribution function or else with a DFT based on the direct-correlation function. All three theoretical approaches reproduce the main trends fairly well, but exhibit inconsistent accuracy, particularly for attractive particle-particle interactions. We show that the wall-particle and particle-particle attractions can couple together to induce a nonlinear enhancement of the adsorption and a related "repulsion through attraction" effect for the effective wall-wall forces. We also investigate the phenomenon of bridging, where an attractive wall-particle interaction induces strongly attractive solvation forces. © *2008 American Institute of Physics*.
[DOI: 10.1063/1.2921134]

I. INTRODUCTION

The interaction between two surfaces in solution can be qualitatively modified by the presence of smaller suspended particles.[1–7] For example, charged co- and counterions will screen any charged groups, and the addition of nonadsorbing polymer can lead to attractive depletion interactions, as first explained over 50 years ago by Asakura and Oosawa.[8] In this paper, we study the effective solvation force between two planar walls in a slit pore geometry, induced by a bath of monodisperse spherical particles that are in osmotic equilibrium with a reservoir of spherical particles at the same chemical potential. Although this model is much simpler than a typical physical system, where the surfaces are heterogeneous and many different particle species are simultaneously in solution, it nevertheless exhibits some remarkably complex behavior, and has therefore been extensively studied.[9–25]

The potentials induced for the two plate geometry can also be related to the force induced between two spheres through the Derjaguin approximation,[1,26] which increasingly becomes accurate for larger size asymmetries. Just as for the case of two plates, most early work on the effective interactions between spheres, induced by the addition of smaller particles, focused on hard-core interactions[27,28] which generally lead to attractive solvation forces, although repulsive oscillations occur with increasing packing fraction of the smaller particles.[29,30] More recently, an increasing number of studies have gone beyond these simpler hard-core depletion models, see, e.g., Refs. 31–35 and references therein. Adding attractive or repulsive interactions leads to considerably more complex behavior, including repulsive solvation forces that can stabilize colloidal suspensions through a nanoparticle halo mechanism, as suggested by the experiments of Lewis *et al.*[36,37] and later explained by computer simulations[38] and hypernetted chain (HNC) integral equations.[39]

One difficulty in understanding the effects of adding these more sophisticated interactions is that the number of different parameters to vary, e.g., the magnitude and range of the attractions/repulsions, etc., becomes quite large, making an analysis of the problem complex. An advantage of the two wall geometry over the two-colloid geometry is that the size ratio between the big and small particles is no longer a variable, simplifying the analysis.

Another advantage of the two plate geometry is that density functional theory (DFT) is easier to apply to this one-dimensional problem than to the more complex cylindrical symmetry of the two-colloid geometry. By using the clever method of Roth *et al.*,[40] the two-colloid problem can be reduced to much simpler one-dimensional integrals, but for this one needs a good *two-component* DFT. While the fundamental measure theory (FMT) provides such a functional for hard-core interactions[41,42] and can be extended to nonadditive HS mixtures[43,44] and soft-core repulsions,[45] no two-

a)Electronic mail: ard.louis@physics.ox.ac.uk.

component theory of comparable accuracy exists for more general interactions.

In this paper, we perform grand canonical Monte Carlo (GCMC) computer simulations for the two-plate geometry, using the same set of interactions as in an earlier systematic study of effective forces induced by smaller colloids of diameter σ between two larger colloids of diameter 5σ.[35] These simulations are then compared to HNC integral equations, which are easy and fast to use, but for which the reliability in this geometry is not always known *a priori*. We also compare the simulations to two different methods to extend FMT-DFT when the particle-particle interactions include additional Yukawa attractions or repulsions: (1) a perturbative method based on the radial distribution function (RDF) that reduces to thermodynamic perturbation theory in the homogeneous limit,[46] and (2) a recent proposal by Tang and Wu,[47] that expands in the direct-correlation function (DCF), and which is based on an earlier proposal by Rosenfeld.[48] In general, we find that the Wu–Tang DFT is an improvement over the RDF perturbation method in the regime we investigate, but all three theoretical methods—integral equations and the two DFTs—still have some difficulty for systems with attractive interparticle interactions.

The simplified geometry also allows us to study in more detail the two different effects described earlier for colloidal mixtures:[35,39] First, strong enough wall-particle attractions can lead to very large attractive forces between the plates when both walls interact with the same set of particles. This phenomenon is known as *bridging*,[1,2] and we show how it can be qualitatively understood from a very simple ideal particle model. Second, we study in more detail the "repulsion through attraction" effect first described in Ref. 35, where the combined effect of wall-particle and particle-particle attractions can lead to an enhancement of the adsorption at a single wall and a concomitant repulsion between the two plates.

We proceed as follows: In Sec. II, we describe our model parameters in more details; in Sec. III, we explain how we performed our GCMC simulations, describe our approach to solving the HNC integral equations as well as the two DFT methods we employ. In Sec. IV, we present our results for the density profiles near a single wall as well as the effective induced forces between the two plates, comparing them to HNC and DFT calculations. In Sec. V, we provide some examples of the nonlinear enhancement effect and the related repulsion through attraction behavior of the forces. Finally, in Sec. VI, we demonstrate some examples of bridging attraction, and in the Appendix provide a simple analytical model that helps explain the basic physics behind bridging.

II. MODEL

The interactions between the spherical particles are modeled as hard-core Yukawa potentials, as in Ref. 35:

$$u_{pp}(r) = \begin{cases} \infty, & r < \sigma \\ \phi_{pp}(r), & r \geqslant \sigma, \end{cases} \tag{1}$$

where r denotes the distance between the centers of the particles, and $\phi_{pp}(r)$ is

TABLE I. Parameter combination.

Run	$\beta\epsilon_{wp}$	$\beta\epsilon_{pp}$
1	0	0
2	0	2.99
3	0	−0.996
4	0.82	0
5	0.82	2.99
6	0.82	−0.996
7	−0.82	0
8	−0.82	2.99
9	−0.82	−0.996

$$\phi_{pp}(r) = \frac{\epsilon_{pp}\sigma}{r} \exp[-\kappa_{pp}(r-\sigma)]. \tag{2}$$

Similarly, the wall-particle interaction is given by

$$u_{wp}(z) = \begin{cases} \infty, & z < \dfrac{\sigma}{2} \\ \phi_{wp}(z), & z \geqslant \dfrac{\sigma}{2} \end{cases} \tag{3}$$

where

$$\phi_{wp}(z) = \epsilon_{wp} \exp\left[-\kappa_{wp}\left(z - \frac{\sigma}{2}\right)\right], \tag{4}$$

and z is the distance of the center of the particle from the wall. This is equivalent to the hard-core Yukawa big-small interaction from Ref. 35, but in the limit of infinite size ratio.

Even with the fairly simple and flexible Yukawa model, there are many different parameters to vary. To simplify our analysis, we keep the following fixed to the same values as in Ref. 35: The packing fraction of the small particles is set to $\eta = \pi\rho_b\sigma_{pp}^3/6 = 0.1$, with ρ_b being the bulk density, while the ranges are given by $\kappa_{wp} = 1.2/\sigma$ and $\kappa_{pp} = 3.0/\sigma$. The range of the wall-particle interaction is of the order of the particle size, while the range of the particle interaction is less than the particle size.

In total, we studied nine different interactions by varying $\beta\epsilon_{pp}$ and $\beta\epsilon_{wp}$ such that each is either positive, negative, or zero. The detailed values are the same as those in Ref. 35 and are given in Table I.

III. METHODS

A. Computer simulations

To investigate the effective forces induced by the particles on the two walls, we performed GCMC simulations[49] at different wall separations L to determine the particle density profile. The bulk packing fraction (for $L=\infty$) was set to $\eta = 0.1$, by first performed an NVT simulation on a bulk system of $N = 500$ particles with periodic boundary conditions in all directions. The Widom particle insertions method[49] was used to determine the chemical potential μ for $\eta = 0.1$.

The production GCMC runs were then performed for a geometry with two parallel walls at a given separation L along the z axis. In the x and y directions, periodic boundary conditions were used, and the size of the plates $L_x = L_y$ was

determined by the condition of having at least 200 particles in the simulation box at equilibrium, so as to minimize finite size effects. These two plate sizes are usually found after a few trial runs and are a bit harder to find when $L=1.05\sigma$, the smallest separation that we simulate. They also vary with the system, i.e., the chemical potential, the wall-particle interaction, and L. On average, we performed on the order of 10×10^6 MC trial moves per particle to equilibrate and gather statistics. For each separation L, we calculated the density profile of the particles between the two walls, $\rho^L(z)$, from which the effective induced force per unit area can be calculated:

$$\frac{\beta F^{\text{eff}}(L)}{\sigma^2} = \rho^L\left(\frac{\sigma}{2}\right) + \int_{\sigma/2}^{L-\sigma/2} \rho^L(z)\left(-\frac{d\beta\phi_{wp}(z)}{dz}\right)dz, \quad (5)$$

where the first term arises from the discontinuity in the derivative of the hard-core wall-particle interaction.

B. Integral equations

In order to calculate the density profile of an inhomogeneous fluid with integral equations, we use the singlet Ornstein–Zernike equation[46]

$$h(z) = c(z) + \rho_b \int d\vec{r}\,' h(z')c_b(|\vec{r}-\vec{r}\,'|), \quad (6)$$

where $c_b(r)$ is the DCF of the bulk fluid, $h(z)$ the wall-particle total correlation function, and $c(z)$ is the wall-particle direct-correlation function. A number of different closures could be used to complete the equations above. In this paper, we use the HNC approximation because we found it to be the most consistently accurate closure for highly asymmetric binary colloid mixtures.[50] For the wall-particle geometry, the HNC approximation reads

$$h(z) - c(z) = \ln[h(z)+1] + \beta u_{wp}(z), \quad (7)$$

where the only spatial coordinate is z, the distance from the wall. The former two relations bring us to

$$h(z) = \exp\left[-\beta u_{wp}(z) + \rho_b \int d\vec{r}\,' h(z')c_b(|\vec{r}-\vec{r}\,'|)\right] - 1, \quad (8)$$

which is iteratively solved to find $h(z)$. Here, the direct-correlation function of the bulk $c_b(r)$ is also found in the HNC approximation (but it could also come from a different approach).

A further HNC approximation can be made,[51] such that the solvent mediated excess interaction free energy per unit area (effective potential per unit area) between two walls at distance z is given by

$$\frac{\beta V^{\text{eff}}(z)}{\sigma^2} = -\rho_b \int_{-\infty}^{\infty} h(s)c(z-s)ds, \quad (9)$$

where $h(s)$ and $c(s)$ are the total and direct wall-particle correlation functions, respectively. The solvation force follows from the equation above as

$$\beta F^{\text{eff}}(z) = -\frac{d\beta V^{\text{eff}}(z)}{dz}. \quad (10)$$

In the analysis above, the wall-wall bridge function in Eq. (9), the wall-particle bridge function in Eq. (7), and the particle-particle bridge function in calculating the bulk DCF $c_b(r)$, are all omitted, so that this is equivalent to a HNC approximation in all three steps.

C. Density functional theory

FMT-DFT (Ref. 41) has emerged as one of the most powerful theoretical techniques to study HS fluids in confined geometries. We adopt the very accurate "White Bear" version[42] which can be written as

$$F[\rho(\vec{r})] = F_{id}[\rho(\vec{r})] + F_{\text{FMT}}[\rho(\vec{r})] + F_w[\rho(\vec{r})] + F^{\text{pert}}[\rho(\vec{r})], \quad (11)$$

where the ideal contribution is exactly given by

$$F_{id}[\rho(\vec{r})] = k_BT \int d\vec{r}\rho(\vec{r})[\ln(\Lambda_s^3(\vec{r})) - 1] \quad (12)$$

and Λ_s is a particle length scale. The FMT HS contribution is of the "weighted density" type, namely,

$$\beta F_{\text{FMT}}[\rho_b] = \int d\vec{r}[\Phi_1(\{n_j(\vec{r})\}) + \Phi_2(\{n_j(\vec{r})\}) + \Phi_3(\{n_j(\vec{r})\})], \quad (13)$$

where the $n_j(\vec{r})$ are weighted densities of the form

$$n_j(\vec{r}) = \int \omega^{(j)}(\vec{r}-\vec{r}\,')\rho(\vec{r}\,')d\vec{r}\,'. \quad (14)$$

Further details of the functions Φ_i and weight functions $w^{(j)}(\vec{r})$ can be found in Refs. 41 and 42. The fluid-wall interaction is taken into account by the external field term:

$$F_w[(\vec{r})] = \int_0^L \rho(r)[\phi_{wp}(z) + \phi_{wp}(L-z)]). \quad (15)$$

Moreover, in the case where $\epsilon_{pp}\neq0$, i.e., for non-HS interactions, the final term, F^{pert}, in Eq. (11) can be treated in two ways:

(1) The effect of additional non-HS interaction can be approximated by a perturbation theory in the RDF which takes the following form:

$$F^{\text{pert}}[\rho(\vec{r})] = \int d\vec{r}\rho(\vec{r})\Psi_1(\vec{r}), \quad (16)$$

where the interactions are taken into account through

$$\Psi_1(\vec{r}) = \frac{1}{2}\int d\vec{r}\,'\rho(\vec{r}\,')\phi_{pp}(|r-r'|)g_{\text{HS}}(|r-r'|,\bar{\rho}(\vec{r},\vec{r}\,')). \quad (17)$$

Here $g_{\text{HS}}(r)$ is the RDF for homogeneous reference system. It is evaluated at an intermediate density between the two points $\vec{r}$ and $\vec{r}\,'$:

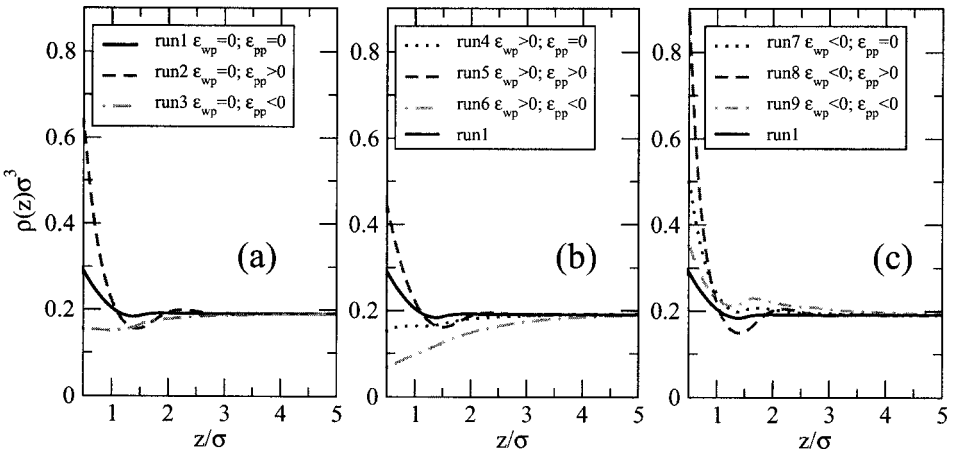

FIG. 1. [(a)–(c)] Density profiles of the centers of the particles as a function of the distance z from the surface of a single wall. Results are from simulations and $\beta\epsilon_{wp}$ and $\beta\epsilon_{pp}$ are varied. The values of $\beta\epsilon_{ij}$ can be found in Table I.

$$\bar{\rho} = \frac{\bar{\rho}_\nu(\vec{r}) + \bar{\rho}_\nu(\vec{r}')}{2}, \tag{18}$$

with

$$\bar{\rho}_\nu(\vec{r}) = \frac{3}{4\pi R_\nu^3} \int_{|r-r'|<R_\nu} \rho(\vec{r}')d\vec{r}'. \tag{19}$$

$\bar{\rho}_\nu(\vec{r})$ is a smoothed density profile around $\vec{r}$; the radius R_ν is of the order of $\sigma/2$, and results are not expected to be very sensitive to the precise value of R_ν. Here, we follow Ref. 52 and choose $R_\nu=0.8\sigma$.

(2) In a recent paper,[47] Tang and Wu proposed a new DFT (based on an earlier suggestion by the late Yasha Rosenfeld[48]) to perturb around the FMT solution by expanding in the attractive component of the DCF that follows from the Yukawa terms, an approach in the spirit of the mean-spherical approximation.[46] In this case, the perturbative contribution of the free energy functional is given by

$$F^{\text{pert}}[\rho(\vec{r})] = F^{\text{pert}}(\rho_b) + \mu^{\text{pert}} \int \Delta\rho(\vec{r})d\vec{r} - \frac{1}{2}\int c_1(\vec{r}-\vec{r}')\Delta\rho(\vec{r})\Delta\rho(\vec{r}')d\vec{r}d\vec{r}', \tag{20}$$

where $\Delta\rho(\vec{r})=\rho(\vec{r})-\rho_b$, $F^{\text{pert}}(\rho_b)$, and μ^{pert} are, respectively, the perturbative parts of the bulk free energy and the excess chemical potential, and $c_1(\vec{r})$ is the first-order contribution of the Yukawa DCF, which can be analytically calculated using the first-order mean-spherical approximation.[47]

IV. RESULTS

A. Density profiles

Before studying the solvation force between two plates, we first examine the trends that the density profile $\rho(z)=\rho_b(h(z)+1)$ of particles at a single wall follows as the wall-particle and particle-particle interactions are changed.

In Fig. 1(a), the density profiles for runs 1–3 are shown. In these runs, there is only a hard wall-particle interaction, i.e., $\beta\epsilon_{wp}=0$. Adding an additional repulsive particle-particle interaction results in increased accumulation near the wall, whereas the addition of an attractive interaction has the opposite effect.

In Fig. 1(b), the density profiles for runs 4–6 are shown. In these runs there is a repulsive wall-particle interaction with $\beta\epsilon_{wp}=0.82$. As expected, this repulsion results in a reduction of the density near the wall, when compared to the case with only a hard wall-particle interaction. Again, the particle-particle repulsion enhances the contact density, whereas the attraction leads to its further depletion.

In Fig. 1(c), the density profiles for runs 7–9 are shown. In these runs there is an attractive wall-particle interaction with $\beta\epsilon_{wp}=-0.82$, leading to an enhancement of the contact density. As in the previous cases, adding an extra particle-particle repulsion increases the contact density. However, in contrast to the other cases where the mutual attraction of the particles leads to an overall depleted density profile with respect to hard particle case, here we observe significant regions where there is an enhanced accumulation of particles next to the wall. Although the contact density is smaller than in run 7, there is a larger secondary maximum further out, which denotes a second layer of particles. Thus, the relative adsorption of particles to the wall is larger than in the case where there is no mutual particle attraction. The reasons for this nonlinear enhancement of the particle densities will be discussed further in Sec. V.

For the runs above, the interaction between the wall and the particles plays the dominant role in determining the shape of the density profile. Adding mutual repulsion between the particles enhances the contact density, and this can be qualitatively understood by mapping the repulsive particles to effective HS particles with a larger effective diameter and hence larger effective packing fraction. The effect of the mutual attraction of the particles can be understood by the fact that the particles prefer the bulk over the wall. The exception is Run 9, where the wall-particle attraction enhances the density near the wall, which now attracts a second layer of particles. The trends found here for the $\rho(z)$ are qualitatively similar to those found in an earlier study for the density profiles of small particles around bigger ones for a binary sphere mixture of moderate asymmetry $q=0.2$.[35]

In Fig. 2, we compare the density profiles from simulation with integral equation (HNC) and the two versions of

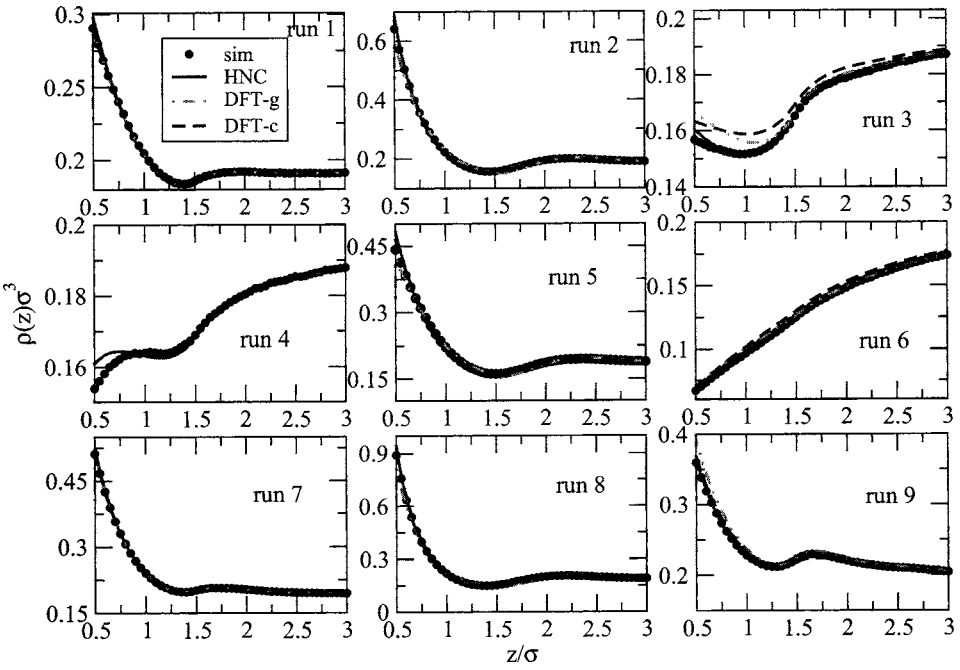

FIG. 2. Density profiles near a single plate for the parameters from Table I. Simulations are compared to HNC integral equation and two versions of DFT. DFT-g represents the perturbation in $g(r)$ and DFT-c a perturbation in $c(r)$.

DFT. DFT-g represents the perturbation in $g(r)$ and DFT-c represents the Tang-Wu[47] DFT with a perturbation in $c(r)$. For runs 1, 4, and 7, with pure HS particle-particle interactions, the DFTs both reduce to HS FMT which is quantitatively accurate, as expected.[42] Their performance is also excellent for repulsive particle-particle interactions. The worst performance is for attractive particle-particle interactions. Overall, no one method is clearly superior to the others, although we do expect the DFTs to be better than HNC at higher packing fractions.

B. Effective solvation forces

In Fig. 3, we compare the effective solvation forces for all nine runs detailed in Table I. They are only depicted in the regime $L \geqslant \sigma$, since for $0 \leqslant L < \sigma$ no particles fit between the plates and the pressure (or solvation force per unit area) is simply $\beta P(L) = \beta F^{\text{eff}}(L)/\sigma^2 = -\beta P_{\text{bulk}}$ (there will typically be a discontinuous jump at $L=\sigma$).

The main trends can be rationalized as follows: When the density profile shows an accumulation of particles near the wall, we expect to find repulsive forces because of the work needed to squeeze the layer of the particles out when the two walls approach one another. On the other hand, when the region next to a wall is depleted of particles, we expect to find attractive forces. Thus run 4, with $\beta\epsilon_{wp} > 0$, results in a more attractive interaction than run 1, where there are only HS repulsions. Similarly run 7, with $\beta\epsilon_{wp} < 0$, generates a more repulsive effective force. The addition of repulsion be-

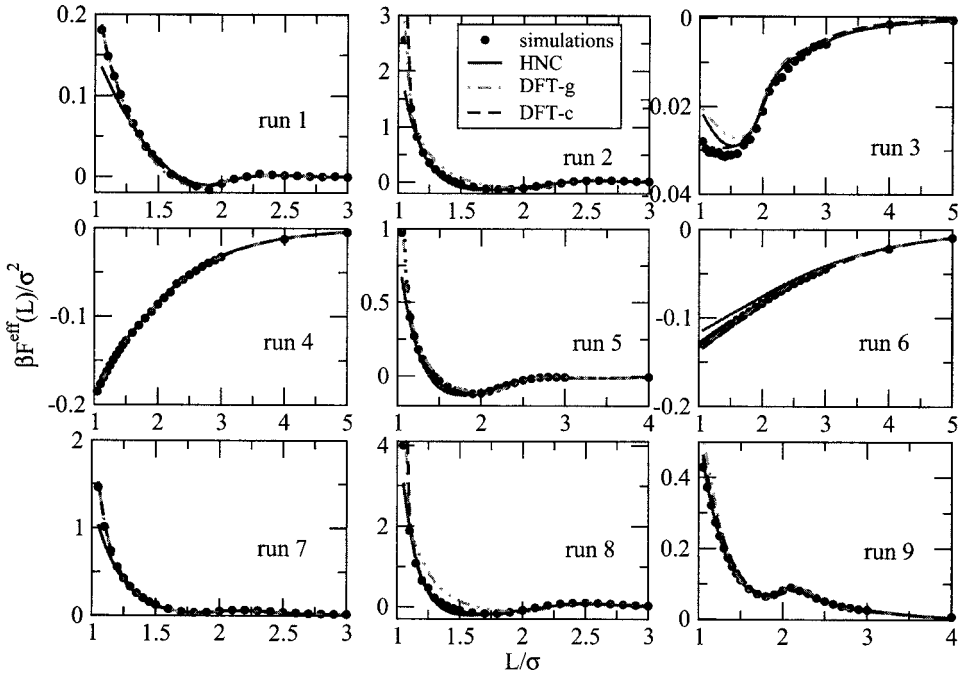

FIG. 3. Effective solvation force per unit area between two plates in the range $L \geqslant \sigma$, for the parameters from Table I. Simulations are compared to HNC integral equation and two versions of DFT. DFT-g represents the perturbation in $g(r)$ and DFT-c a perturbation in $c(r)$. (Note that the scales are not the same in each graph, but rather are adjusted to enhance comparison between simulation and the theoretical techniques.)

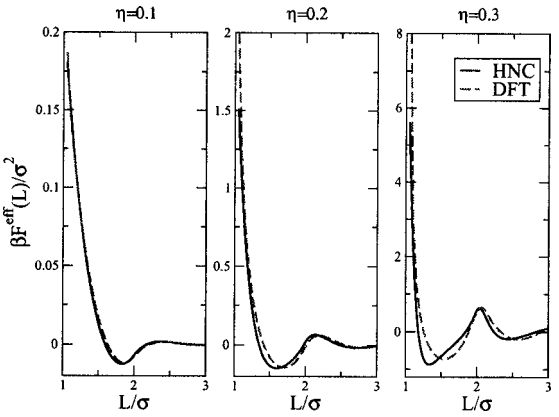

FIG. 4. Solvation force per unit area (or equivalently the solvation pressure) between two plates in the range $L \geqslant \sigma$, for pure HS systems: A comparison between FMT-DFT (Ref. 41), which is expected to be virtually indistinguishable from simulations in this regime (Ref. 42), and HNC, which shows deviations for increasing packing fractions.

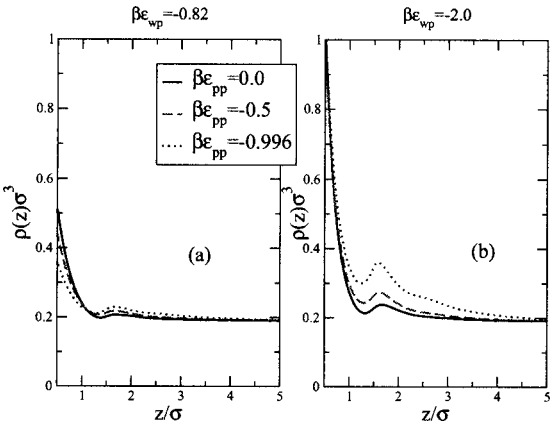

FIG. 5. GCMC simulations of density profiles for two different wall-particle attractions. With increasing particle-particle attraction, the secondary maximum is enhanced when the wall-particle attraction is stronger.

tween the particles ($\beta\epsilon_{pp}>0$) is equivalent to an effective enhancement of the packing fraction which in turn accounts for the more pronounced oscillations. On the other hand, when the particles are attractive ($\beta\epsilon_{pp}<0$), the picture is slightly more complex due to the possibility of nonlinear couplings which are discussed further in Sec. V.

In Fig. 3, we compare the performance of HNC integral equations as well as our two versions of DFT for the solvation force per unit area between the two plates (or equivalently the solvation force). The trends are similar to those found for the density profiles in Fig. 2: For pure HS particles the DFT and simulation are the same to within simulation errors; for an additional repulsive particle-particle interaction, the DFT-*c*, based on the direct-correlation function, slightly performs better than the DFT-*g* based on the RDF. All three methods show the worst performance for attractive particle-particle interactions, although here again the DFT-*c* is slightly better than the other methods. Overall, the performance of all three methods is encouraging. We expect deterioration of the performance for all three theoretical methods when the system is close to a fluid-fluid spinodal line.[46] We also expect the HNC integral equation technique to perform less well at higher packing fractions. A measure of this can be seen in Fig. 4 where HNC is compared to FMT DFT, which is expected to be quantitatively accurate at these densities.[42] How the two DFTs work at higher packing fractions when attractive or repulsive interactions are added remains to be more fully investigated.

V. REPULSION THROUGH ATTRACTION

Figures 2 and 3 both showed, particularly for run 9, that adding an attractive particle-particle interaction could result in an enhanced density profile or a more repulsive solvation force when combined with an attractive wall-particle interaction. This nonlinear coupling effect was also noted in Ref. 35, and for cases where it led to enhanced effective repulsive forces, it was named a repulsion through attraction effect.

To investigate this phenomenon further, we performed simulations varying both $\beta\epsilon_{wp}$ and $\beta\epsilon_{wp}$, and show the results for the density profile in Fig. 5, and for the pressure or solvation force in Fig. 6. For $\beta\epsilon_{wp}=-0.82$, making the particle-particle attraction stronger enhances the secondary maximum in the density profile, while it decreases the contact value. This means that it is more favorable for the particles to be in the second layer than in the first next to the wall or in the bulk. The effective solvation forces per unit area follow similar trends as the density. For a higher wall-particle attraction, $\beta\epsilon_{wp}=-2.00$, the enhancement of the secondary maximum of the density profile is more dramatic and the contact value remains almost the same. The solvation force is also enhanced due to the attractive particle-particle interactions. The wall-particle attraction enhances the particle-particle attraction effect through a nonlinear coupling, resulting in the repulsion through attraction effect also signaled in Ref. 35

Another measure for the nonlinear coupling between wall-particle and particle-particle interactions is the reduced adsorption defined as

$$\hat{\Gamma} = \frac{\Gamma}{\rho_b} = \frac{1}{\rho_b}\int_0^\infty (\rho(z) - \rho_b)dz, \tag{21}$$

where $\rho(z)$ is the particle density at a single wall. In Fig. 7, we plot the reduced adsorption as a function of the intensity

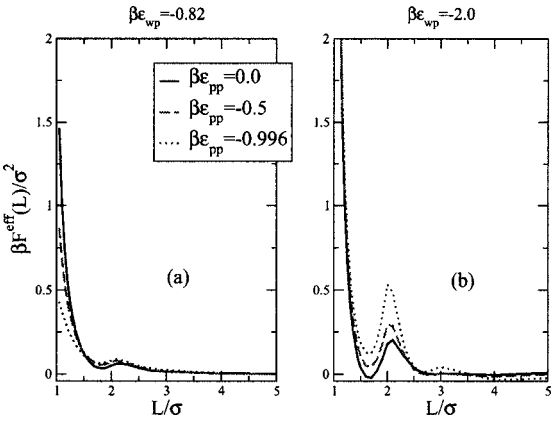

FIG. 6. GCMC simulations of effective solvation forces per unit area for two different wall-particle attractions. With increasing particle-particle attraction, the secondary maximum is enhanced when wall-particle attraction is stronger, an effect called repulsion through attraction.

of the particle-particle interaction. These lines were calculated with HNC, which we expect to be accurate enough to faithfully reproduce the right trends for these parameters.

When $\epsilon_{pp}>0$ [Fig. 7(b)], the reduced adsorption is generally an increasing function of ϵ_{pp}, although there may be a local minimum at small ϵ_{pp}. The reason for this is that increasing ϵ_{pp} increases the pressure from the bulk onto the interfacial region, which generally increases the adsorption.

When, on the other hand, $\epsilon_{pp}<0$ [Fig. 7(a)] and the wall-particle attraction is relatively weak, then the reduced adsorption decreases with increasing particle-particle attraction, the reason being that the particles now prefer to be in the bulk fluid rather than at the interface. For stronger wall-particle attractions, however, a different effect occurs, and we observe a strong increase in the reduced adsorption $\hat{\Gamma}$ above a certain threshold value of ϵ_{pp}. This is caused by a nonlinear coupling: the strong wall-particle attraction enhances the number of particles near the wall, and this in turn attracts increasing numbers of other particles. Although we only plot results for one density ($\eta=0.1$), we find that in general, the higher the density of the system, the stronger the wall-particle attraction should be in order to see this transition in the slope. While it can be proved that $\partial\Gamma/\partial\epsilon_{wp}<0$, irrespective of the particle-particle interactions,[53] from the graphs it is clear that $\partial\Gamma/\partial\epsilon_{pp}$ can be either negative or positive.

VI. BRIDGING

When two surfaces are attracted to the same set of small particles, a large attractive effective interaction between the surfaces can result. This effect is sometimes called bridging attraction. It commonly occurs, for example, with polymers that are attracted to surfaces. In a previous study, we also observed this effect for binary colloidal mixtures.[39] Here we study bridging for the two wall geometry.

In Fig. 8, we plot the effective potential calculated with the wall-HNC method for different intensities of wall-particle attraction $\beta\epsilon_{wp}$. The bulk system is that of run 2. For small attraction, the effective solvation force becomes more repulsive, but as $\beta\epsilon_{wp}$ becomes increasingly attractive, we observe the appearance of a new minimum that rapidly increases with larger wall-particle attractions. This attractive minimum asymptotically moves toward a separation of one particle diameter $L=1\sigma$, signaling that the two plates are attracted by the same set of particles.

The qualitative features observed in Fig. 8 can be reproduced by considering the simpler ideal fluid limit, for which the particle-particle interactions are set to zero.[54] If the ideal fluid is confined between two walls in separation L then the external potential is given by

$$u_{\text{ext}}(z)=u_{wp}(z)+u_{wp}(L-z), \tag{22}$$

and the normalized density profile is

$$\frac{\rho(z)}{\rho_b}=\exp[-\beta u_{\text{ext}}(z)]. \tag{23}$$

In this limit, the effective potential can then be written as[9]

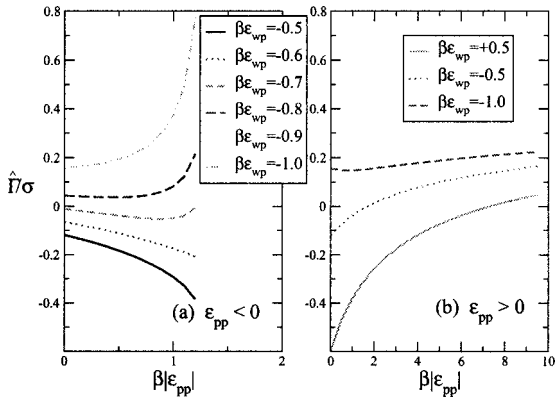

FIG. 7. Reduced adsorption $\hat{\Gamma}$ for (a) attractive particle-particle interactions and (b) repulsive particle-particle interactions.

$$\frac{\beta V^{\text{eff}}(z)}{\sigma^2}=\Gamma(\infty)-\Gamma(z), \tag{24}$$

where

$$\Gamma(z)=\int_0^z(\rho(s)-\rho_b)ds \tag{25}$$

is the adsorption of particles between the two walls. (If there is no particle-wall interaction, then for these ideal particles $\Gamma(z)=0$.) In Fig. 9, we plot the effective potential (divided by the density—because this scales out), for various intensities of the same wall-particle attraction used in Fig. 8. The same nonmonotonic behavior is qualitatively reproduced by an ideal fluid. The two walls mainly repel for weak wall-particle attraction, and this repulsion is initially enhanced as the intensity of $\beta\epsilon_{wp}$ grows, but then eventually an attractive minimum begins developing and rapidly grows. In the Appendix, we present two exactly solvable models that further explain the bridging features seen in Figs. 8 and 9, and suggest that the minimum eventually scales like $\exp[-\beta n\epsilon_{wp}]$, where the n depends on details of the model.

Finally, the calculations in Fig. 8 were for repulsive particle-particle interactions. For attractive particle-particle interactions, the overall picture is more complicated, as the repulsion through attraction effect can also kick in. We find that for strong enough wall-particle attractions, eventually bridging sets in, but, for example, there may be several layers attracted to each other, creating more complex effective wall-wall interactions.[50]

VII. CONCLUSIONS

By performing GCMC computer simulations, we have studied the density profiles of spherical particles near single walls, as well as the effective forces induced between two plates by a sea of particles. The parameters were systematically varied away from the better-studied HS model to examine both attractive and repulsive wall-particle and particle-particle interactions.

The dominant effect of wall-particle and particle-particle interactions is fairly straightforward to rationalize in most cases. (1) Adding *wall-particle repulsion* increases the depletion layer near the wall and results in more attractive solva-

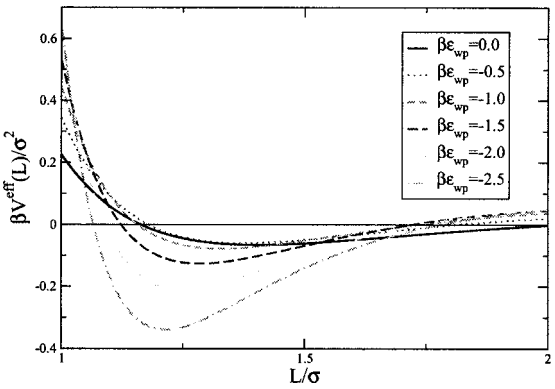

FIG. 8. The effective potential is calculated in the HNC approximation and plotted for various intensities of wall-particle attraction. The bulk system is that of run 2 ($\beta\epsilon_{ss}>0$). The walls repel when the attraction is weak but start to attract each other with increasing wall-particle attraction, due to the phenomenon of bridging.

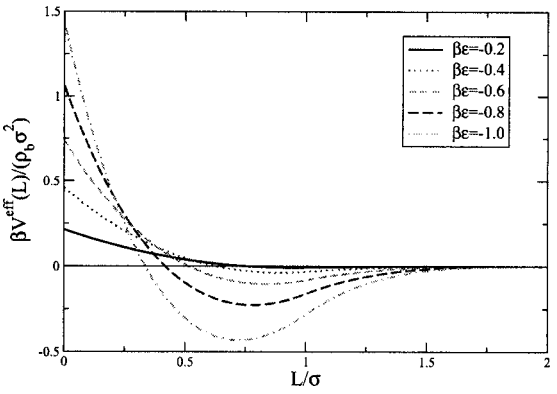

FIG. 10. The quantity $\beta V^{\mathrm{eff}}/(\rho_b\sigma^2)$ is plotted for the ideal fluid at various intensities of the wall-particle triangle-form interaction. The walls repel when the attraction is weak but start to attract for higher attraction, denoting the phenomenon of bridging.

tion forces. (2) Adding *wall-particle attractions* decreases the depletion layer near the wall and leads to more repulsive solvation forces. Similarly, for a fixed wall-particle interaction, (3) adding additional *particle-particle repulsion* can be rationalized in terms of an effective HS model with a larger diameter and packing fraction. (4) Adding additional *particle-particle attractions* tends to deplete particles from the wall as it is more favorable for them to reside in the bulk. In general, the effects of changing wall-particle and particle-particle interactions are, to first order, independent of each other.

For strong wall-particle interactions, however, the above simpler generalizations can break down. One subtle effect occurs when both interactions are sufficiently attractive. Instead of the bulk being more favorable for the particles, the added attraction near the wall leads to an accumulation of particles, which in turn attract more particles from the bulk. The resulting nonlinear coupling effect increases the density near the wall, and may also lead to more repulsive solvation forces, an effect called *repulsion through attraction*.[35]

Strong wall-particle attraction can also induce *bridging forces*,[1,2] where both surfaces are attracted to the same set of particles. This behavior can quite easily be rationalized by studying the simpler ideal particle limit. These attractions

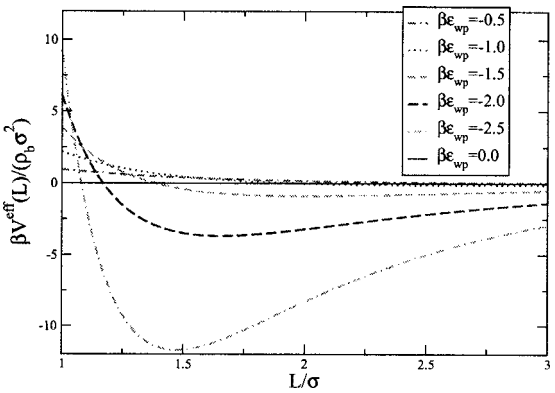

FIG. 9. The effective potential, divided by the density, for the ideal fluid at various intensities of wall-particle attraction ($\kappa_{wp}=1.2/\sigma$). For stronger wall-particle attractions, the phenomenon of bridging is observed.

can become very strong, as observed in Refs. 38 and 39. In the Appendix, we show that in the ideal limit the attractive minimum of the potential can asymptotically grow as a power of $\exp[-\beta\epsilon_{wp}]$, where ϵ_{wp} is a measure of the wall-particle interactions.

Computer simulations, while very accurate, are still rather expensive to perform, and it would be desirable to have accurate theoretical techniques to more rapidly explore the very large parameter space available when both particle density and interactions are varied. We compared the performance of two version of DFT, and the HNC integral equation technique. All three methods performed fairly well, especially for repulsive particle-particle interactions. Performance was slightly less good for attractive particle-particle interactions, with no single method clearly better than the others. We note that we investigated these methods at a packing fraction $\eta=0.1$, which is relevant for colloidal dispersions and biological systems, but is lower than the packing fractions for simple liquids[46] for which these methods were originally devised.

There are many physical situations where the two surface geometry we employ here is relevant.[1–7] Direct connections to the effective interactions induced between two spheres by a sea of smaller particles can also be obtained through the Derjaguin approximation.[26] The advantage of this geometry over the two sphere geometry is that it is generally easier to simulate and also easier to apply theoretical techniques. In the future we hope to study plates with more complex interactions, including heterogeneous surfaces, which are physically relevant, and have been shown to induce complex behavior.[55–57]

ACKNOWLEDGMENTS

S.K. would like to thank Schlumberger Cambridge Research and the EPSRC through IMPACT Faraday for funding during the academic years 2002–2005. J.D. acknowledges financial support by the Deutsche Forschungsgemeinschaft (DFG). A.M.J. thanks the Spanish Ministerio de Educación y Ciencia (Project No. MAT2006-12918-C05-01), The Euro-

pean Regional Development Fund (ERDF), and the Junta de Andalucía (Excellency Project FQM 392). A.A.L. thanks the Royal Society (London) for funding.

APPENDIX: EXACTLY SOLVABLE MODELS FOR BRIDGING IN THE IDEAL FLUID LIMIT

Square well potential

We consider an ideal fluid and assume a wall-particle interaction of the form $u_{wp}(z)=\epsilon$ for $0\leqslant z\leqslant\sigma$ and $u_{wp}(z)=0$ otherwise (square well potential), where $\epsilon<0$ is the intensity of the attraction and σ is the length scale. This model is easy to analytically solve, and Eq. (24) gives

$$\frac{\beta V^{\mathrm{eff}}(L)}{\rho_b\sigma^2}=\begin{cases}2\sigma(e^{-\beta\epsilon}-1)-L(e^{-2\beta\epsilon}-1), & 0\leqslant L\leqslant\sigma\\ (L-2\sigma)(e^{-\beta\epsilon}-1)^2, & \sigma\leqslant L\leqslant 2\sigma\\ 0, & L\geqslant 2\sigma.\end{cases} \tag{A1}$$

This potential has a positive value at contact and a negative minimum of $-\sigma(e^{-\beta\epsilon}-1)^2$ at $L=\sigma$, which both monotonically grow increasing wall-particle attraction. The negative well is typical of bridging behavior. For large attraction the minimum scales as $\beta V^{\mathrm{eff}}(\sigma)/\sigma^2\sim-\rho_b\sigma e^{-\beta 2\epsilon}$. Its simple Boltzmann factor form can be qualitatively understood as the free-energy gain emerging from a number density ρ_b of particles interacting with both walls.

Triangle potential

We now move up one step further in complexity and consider a wall-particle interaction of the form $u_{wp}(z)=\epsilon-(\epsilon/\sigma)z$ for $0\leqslant z\leqslant\sigma$ and $u_{wp}(z)=0$ otherwise (triangle potential), where $\epsilon<0$ is the intensity of the attraction and σ is the length scale. This model is also easy to analytically solve, and Eq. (24) gives

$$\frac{\beta V^{\mathrm{eff}}(L)}{\rho_b\sigma^2}=\begin{cases}\dfrac{2\sigma}{\beta\epsilon}(1-e^{-\beta\epsilon}-\beta\epsilon)-L(e^{-2\beta\epsilon+\beta\epsilon/\sigma L}-1), & 0\leqslant L\leqslant\sigma\\ 2e^{-\beta\epsilon}\dfrac{\sigma}{\beta\epsilon}(e^{\beta\epsilon}-e^{\beta\epsilon/\sigma(L-\sigma)})-(2\sigma-L)(e^{-2\beta\epsilon+\beta\epsilon/\sigma L}+1), & \sigma\leqslant L\leqslant 2\sigma\\ 0, & L\geqslant 2\sigma.\end{cases} \tag{A2}$$

In Fig. 10, we plot the dimensionless effective potential for various $\beta\epsilon$. For small wall-particle attraction the walls mainly repel, but when the attraction becomes stronger a minimum begins to grow in the first branch $L\leqslant\sigma$, which becomes deeper with larger values of $|\beta\epsilon|$ eventually scaling as $-e^{-2\beta\epsilon}/\beta\epsilon$ in the limit $\beta\epsilon\rightarrow-\infty$. The similarities between Fig. 10 and Figs. 8 and 9 suggests that the basic physics of bridging is already captured by this very simple triangle model.

[1] J. N. Israelachvili, *Intermolecular and Surface Forces* (Academic, London, 1992).
[2] W. B. Russel, D. A. Saville, and W. R. Schowalter, *Colloidal Dispersions* (Cambridge University Press, Cambridge, 1989).
[3] P. N. Pusey, in *Liquids, Freezing and the Glass Transition*, edited by J. P. Hansen, D. Levesque, and J. Zinn-Justin (North Holland, Amsterdam, 1991).
[4] L. Belloni, J. Phys.: Condens. Matter **12**, R549 (2000).
[5] D. Leckband and J. Israelachvili, Q. Rev. Biophys. **34**, 105 (2001).
[6] A. A. Louis, Philos. Trans. R. Soc. London, Ser. A **359**, 939 (2001).
[7] C. N. Likos, Phys. Rep. **348**, 267 (2001).
[8] S. Asakura and F. Oosawa, J. Chem. Phys. **22**, 1255 (1954).
[9] R. Evans and U. M. B. Marconi, J. Chem. Phys. **86**, 7138 (1987).
[10] A. Olesky and J. P. Hansen, Mol. Phys. **104**, 2871 (2006).
[11] J. Yi, S. Kim, J. Chem. Phys. **107**, 8147 (1997).
[12] S. Zhou, J. Phys. Chem. B **106**, 7674 (2002).
[13] W. Olivares-Rivas, L. Degreve, D. Henderson, and J. Quintana, J. Chem. Phys. **106**, 8160 (1997).
[14] B. Götzelmann and S. Dietrich, Phys. Rev. E **55**, 2993 (1997).
[15] R. Roth, R. Evans, A. Lang, and G. Kahl, J. Phys.: Condens. Matter **14**, 12063 (2002).
[16] I. K. Snook and D. Henderson, J. Chem. Phys. **68**, 2134 (1978).
[17] R. D. Groot, N. M. Faber, and J. P. van der Eerden, Mol. Phys. **62**, 861 (1987).
[18] J. Forsman, C. E. Woodward, and B. Jonsson, Langmuir **13**, 5459 (1997).
[19] I. K. Snook and W. van Megen, J. Chem. Phys. **70**, 3099 (1979).
[20] D. E. Sullivan, D. Levesque, and J. J. Weiss, J. Chem. Phys. **72**, 1170 (1980).
[21] P. Gonzalez-Mozuelos and J. M. Mendez-Alcaraz, Phys. Rev. E **63**, 021201 (2001).
[22] D. E. Sullivan and G. Stell, J. Chem. Phys. **69**, 5450 (1978).
[23] J. P. Noworyta, D. Henderson, and S. Sokolowski, Mol. Phys. **96**, 1139 (1999).
[24] I. K. Snook and W. van Megen, J. Chem. Phys. **72**, 2907 (1980).
[25] M. Plischke and D. Henderson, J. Chem. Phys. **84**, 2846 (1986).
[26] B. V. Derjaguin, Kolloid-Z. **69**, 155 (1934).
[27] S. Asakura and F. Oosawa, J. Polym. Sci. **33**, 183 (1958).
[28] A. Vrij, Pure Appl. Chem. **48**, 471 (1976).
[29] J. Y. Walz and A. Sharma, J. Colloid Interface Sci. **168**, 485 (1994).
[30] Y. Mao, M. E. Cates, and H. N. W. Lekkerkerker, Physica A **222**, 10 (1995).
[31] R. Garibay-Alonso, J. M. Mendez-Alcaraz, and R. Klein, Physica A **235**, 159 (1997).
[32] S. Amokrane, J. Chem. Phys. **108**, 7459 (1998).
[33] J. Malherbe and S. Amokrane, Mol. Phys. **97**, 677 (1999).
[34] S. A. Egorov and E. Rabani, J. Chem. Phys. **15**, 617 (2001).
[35] A. A. Louis, E. Allahyarov, H. Löwen, and R. Roth, Phys. Rev. E **65**, 061407 (2002).
[36] V. Tohver, J. E. Smay, A. Braem, P. V. Braun, and J. A. Lewis, Proc. Natl. Acad. Sci. U.S.A. **98**, 8950 (2001).
[37] V. Tohver, A. Chan, O. Sakurada, and J. A. Lewis, Langmuir **17**, 8414 (2001).
[38] J. Liu and E. Luijten, Phys. Rev. Lett. **93**, 247802 (2004); Phys. Rev. E **76**, 061401 (2005); S. A. Barr and E. Luijten, Langmuir **22**, 7152 (2006).

[39] S. Karanikas and A. A. Louis, Phys. Rev. Lett. **93**, 248303 (2004).
[40] R. Roth, R. Evans, and S. Dietrich, Phys. Rev. E **62**, 5360 (2000).
[41] Y. Rosenfeld, Phys. Rev. Lett. **63**, 980 (1989); J. Chem. Phys. **98**, 8126 (1993).
[42] R. Roth, R. Evans, A. Lang, and G. Kahl, J. Phys.: Condens. Matter **14**, 12063 (2002); X. Y. Yu and J. Z. Wu, J. Chem. Phys. **117**, 10156 (2002).
[43] A. A. Louis and R. Roth, J. Phys.: Condens. Matter **13**, L777 (2001).
[44] R. Roth, R. Evans, and A. A. Louis, Phys. Rev. E **64**, 051202 (2001).
[45] M. Schmidt, Phys. Rev. E **62**, 3799 (2000).
[46] J. P. Hansen and I. R. McDonald, *Theory of Simple Liquids*, 2nd ed. (Academic, London, 1986).
[47] Y. Tang and J. Wu, Phys. Rev. E **70**, 011201 (2004).
[48] Y. Rosenfeld, J. Chem. Phys. **98**, 8126 (1993).
[49] D. Frenkel, B. Smit, *Understanding Molecular Simulation* (Academic, New York, 2002).
[50] S. Karanikas, Ph.D. thesis, Cambridge University, 2007; S. Karanikas and A. A. Louis (unpublished).
[51] P. Attard, D. R. Berard, C. P. Ursenbach, and G. N. Patey, Phys. Rev. A **44**, 8224 (1991).
[52] S. Sokolowski and J. Fischer, J. Chem. Phys. **96**, 5441 (1992).
[53] R. Roth, personal communication (2003).
[54] J. Forsman, C. Woodward, and B. Freasier, J. Chem. Phys. **118**, 7672 (2003).
[55] E. Allahyarov, H. Löwen, A. A. Louis, and J. P. Hansen, Europhys. Lett. **57**, 731 (2002); E. Allahyarov, H. Löwen, J. P. Hansen, and A. A. Louis, Phys. Rev. E **67**, 051404 (2003).
[56] J. Dzubiella and J. P. Hansen, J. Chem. Phys. **121**, 5514 (2004).
[57] M. O. Khan, S. N. Petris, and D. Y. C. Chan, J. Chem. Phys. **122**, 104715 (2005).